Cardiac automaticity is modulated by I$_{KACh}$ in sinoatrial node during pregnancy

Valérie Long [1,2], Gracia El Gebeily[1,2], Élisabeth Leblanc[1,2], Marwa Senhadji[1,2], and Céline Fiset [1,2]*

[1]Research Center, Montreal Heart Institute, 5000 Bélanger, Montréal, Québec, Canada H1T 1C8; and [2]Faculty of Pharmacy, Université de Montréal, 2940 Chemin de Polytechnique, Montréal, Québec, Canada H3T 1J4

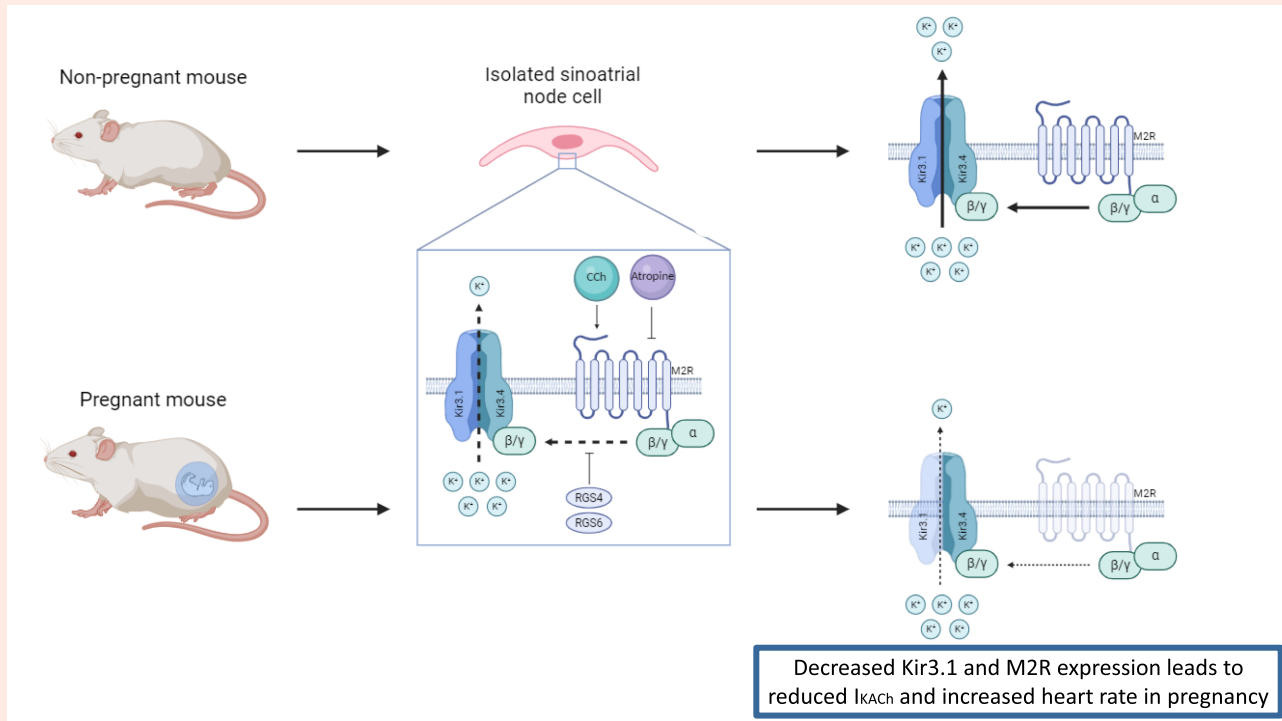|	
Aims	Pregnant (P) women have a significantly elevated resting heart rate (HR), which makes cardiac arrhythmias more likely to occur. Although electrical remodelling of the sinoatrial node (SAN) has been documented, the underlying mechanism is not fully understood. The acetylcholine-activated potassium current (I$_{KACh}$), one of the major repolarizing currents in the SAN, plays a critical role in HR control by hyperpolarizing the maximal diastolic potential (MDP) of the SAN action potential (AP), thereby reducing SAN automaticity and HR. Thus, considering its essential role in cardiac automaticity, this study aims to determine whether changes in I$_{KACh}$ are potentially involved in the increased HR associated with pregnancy.
Methods and results	Experiments were conducted on non-pregnant (NP) and pregnant (P; 17–18 days gestation) female CD-1 mice aged 2 to 4 months. I$_{KACh}$ was recorded on spontaneously beating SAN cells using the muscarinic agonist carbachol (CCh). Voltage-clamp data showed a reduction in I$_{KACh}$ density during pregnancy, which returned to control values shortly after delivery. The reduction in I$_{KACh}$ was explained by a decrease in protein expression of Kir3.1 channel subunit and the muscarinic type 2 receptor. In agreement with these findings, current-clamp data showed that the MDP of SAN cells from P mice were less hyperpolarized following CCh administration. Surface electrocardiograms (ECGs) recorded on anaesthetized mice revealed that the cholinergic antagonist atropine and the selective KACh channel blocker tertiapin-Q increased HR in NP mice and had only a minimal effect on P mice. AP and ECG data also showed that pregnancy is associated with a decrease in beating and HR variability, respectively.
Conclusion	I$_{KACh}$ function and expression are decreased in the mouse SAN during pregnancy, strongly suggesting that, in addition to other electrical remodelling of the SAN, reduced I$_{KACh}$ also plays an important role in the pregnancy-induced increased HR.

---

* Corresponding author. Tel: +(514) 376 3330; fax: +(514) 376 1355, E-mail: celine.fiset@umontreal.ca

Graphical Abstract

Decreased Kir3.1 and M2R expression leads to reduced I$_{KACh}$ and increased heart rate in pregnancy

1. Introduction

Women undergo major cardiovascular changes throughout their pregnancy.[1] These normal physiological changes are essential to meet the greater physiological demands. For instance, as gestation progresses, resting heart rate (HR) gradually increases by 10–20 bpm to enhance cardiac output.[2] However, this increased HR can lead to the onset or exacerbation of supraventricular arrhythmias,[3–5] compromising the health of the mother and the foetus. Although electrical remodelling of the sinoatrial node (SAN) has been shown to contribute to the increased HR during pregnancy,[6,7] the underlying mechanisms have not yet been fully elucidated. Uncovering these mechanisms is of great importance, given the large proportion of women who will become pregnant (P) in their lifetime, putting them at risk of developing cardiac arrhythmias. Furthermore, nowadays, women have their pregnancy at an older age, which is an additional risk factor for the development of arrhythmias.[3,8]

The SAN is responsible for cardiac automaticity and HR control.[9,10] In a series of studies, we demonstrated that pregnancy in mice is associated with increased HR and vulnerability to supraventricular arrhythmias,[6,7,11,12] as in women. We found that the increased HR was not secondary to changes in autonomic tone, blood pressure, or circulating catecholamine levels.[6] However, we did find a significant increase in the density of the hyperpolarization-activated current (I$_f$)[6] and L-type calcium current (I$_{CaL}$)[7] density in SAN cells from P mice. These results were explained by an enhanced expression of HCN2 and *Cacna1d*, respectively, and partly due to the elevated 17β-oestradiol concentrations found in late gestation.[11]

The acetylcholine-activated potassium current (I$_{KACh}$), also known as the G-protein-gated potassium channel, is one of the main repolarizing currents of the SAN and has an essential role in pacemaking activity.[13] As its name indicates, I$_{KACh}$ is activated following parasympathetic stimulation of the heart by acetylcholine.[14] The latter and other muscarinic agonists, such as carbachol (CCh), bind to the G-protein-coupled muscarinic type 2 receptor (M2R), activating the ion channel composed of Kir3.1 and Kir3.4, also known as GIRK1 and GIRK4, respectively.[15] The opening of the G-protein-activated ion channel allows K$^+$ ions to go through, generating I$_{KACh}$. This ionic current may also be negatively regulated by two regulators of G protein signalling (Rgs) found in the SAN, Rgs4[16] and Rgs6.[17] I$_{KACh}$ plays a key role in cardiac automaticity, as its activation hyperpolarizes the maximal diastolic potential (MDP) of the SAN action potential (AP), leading to a reduction in AP rate and a slowing of HR. Conversely, muscarinic antagonists, commonly used in the treatment of SAN bradycardia,[18] inactivate I$_{KACh}$, resulting in an increase in HR.

Accordingly, in this study, we hypothesize that in addition to the already documented electrical remodelling of the SAN, functional changes in I$_{KACh}$ also contribute to increased SAN automaticity and elevated HR during pregnancy.

2. Methods

2.1 Animals

Non-pregnant (NP; 2–4 months) and P (17–18 gestation days) adult female CD-1 mice were purchased from Charles River (St-Constant, Québec, Canada). All mice had access to sterilized food and water, and all cages were maintained under controlled conditions (12 h light/dark cycle, 21 ± 1°C). All animal experiments were performed in agreement with the Canadian Council on Animal Care (CCAC) (Ottawa, Canada) and approved by the Montreal Heart Institute Animal Care Committee (protocol numbers: 2018-80-06 and 2021-80-02). All procedures performed were also conformed to the guidelines from Directive 2010/63/EU of the European Parliament on the protection of animals used for scientific purposes.

2.2 Mouse SAN cell isolation

Mouse SAN cells were isolated using previously published protocols.[6,7,11] Briefly, mice were anaesthetized with 2% isoflurane and killed by cervical dislocation. The heart was quickly removed and dissected in oxygenated HEPES-buffered Tyrode's solution (4°C) containing (in mM) 140 NaCl, 5.4 KCl, 1 $MgCl_2$, 5 HEPES, 5.5 glucose, and 1 $CaCl_2$, pH 7.4 with NaOH. Isolated SAN tissue was cut into four to five pieces and rinsed twice for 4 min in Ca^{2+}-free Tyrode's solution containing (in mM) 140 NaCl, 5.4 KCl, 0.5 $MgCl_2$, 5 HEPES, 50 taurine, 1.2 KH_2PO_4, pH 6.9 with NaOH [adjusted with 0.1% bovine serum albumin (BSA) and 5.5 mM glucose]. SAN tissues were then transferred to the same Ca^{2+}-free Tyrode's solution supplemented with collagenase type II (236.8 U/mL, Worthington Biochemical Corporation, Lakewood, NJ, USA), elastase (1.9 U/mL, Worthington Biochemical Corporation), protease (1.4 U/mL, Sigma-Aldrich), and $CaCl_2$ (100 μM) for 25–30 min at 35°C. To stop the digestion, SAN tissues were rinsed three times in Kraft-Brühe solution (in mM: 100 K^+ glutamate, 10 K^+ aspartate, 25 KCl, 10 KH_2PO_4, 4 $MgSO_4$, 20 taurine, 4.5 creatine, 20 glucose, 5 HEPES, and 0.1% BSA, pH 7.2 with KOH) for 4 min. SAN tissues were gently triturated with a Pasteur pipette for 2 min. SAN cells were stored at room temperature (RT, 22°C), and cellular electrophysiology experiments were performed up to 4–6 h following isolation.

2.3 Cellular electrophysiology

Freshly isolated SAN cells were placed in a recording chamber (∼200 μL) mounted on an inverted microscope and given 25 min to adhere to the bottom of the bath. Cells were then perfused for 5 min prior to recordings with HEPES-buffered Tyrode's solution. Data acquisition was performed using Axopatch 200B patch-clamp amplifier and DigiData 1440A digitizer (Molecular Devices, Sunnyvale, CA, USA). Data were stored in a microcomputer using pCLAMP 10.3 and pCLAMP 10.7 (Molecular Devices). Patch pipettes were pulled from borosilicate capillary glass (World Precision Instruments, Sarasota, FL, USA) and had a resistance of 3–6 MΩ when filled with intracellular solutions (see below). All recordings were performed at 37°C.

2.3.1 Voltage-clamp recordings

I_{KACh} was recorded using the whole-cell voltage-clamp technique. Pipettes were filled with an internal solution containing (in mM) 135 KCl, 8 NaCl, 2 MgATP, 6.6 Na_2phosphocreatine, 0.1 Na_2GTP, 0.1 $CaCl_2$, 10 HEPES, and 5 EGTA; pH 7.2 was adjusted with KOH. A 500 ms voltage ramp protocol from +50 to −120 mV from a holding potential of −40 mV was imposed to the isolated SAN cells three times: (i) under baseline conditions, (ii) 2–2.5 min after the addition of CCh (10 μM),[19] and (iii) 5 min after washout. I_{KACh} was obtained by subtracting the current recorded with and without CCh. For each condition, the ramp protocol was performed three times and the average recording was used for analysis. Voltage-clamp recordings were low-pass filtered (1 kHz) and digitized (4 kHz). All current amplitudes were normalized to the cell capacitance and expressed as densities (pA/pF).

2.3.2 Current-clamp recordings

Spontaneous APs were recorded using the perforated patch-clamp technique (nystatin: 130 ng/mL) in current-clamp mode as previously described.[6,7,11] Pipettes were filled with an internal solution containing (in mM) 135 K^+ aspartate, 6 NaCl, and 5 HEPES; pH 7.2 was adjusted with KOH. Spontaneous APs were recorded under baseline condition, after the addition of CCh (1 μM),[20,21] and after washout. Analysis was performed on stable spontaneous AP recordings of at least 10 s. The liquid junction potential was not corrected.

2.4 Surface ECGs

Surface electrocardiograms (ECGs) were performed as described previously.[6,7] Mice were anaesthetized with 2% isoflurane. Body temperature was maintained at 37°C using a heating pad. Platinum electrodes positioned subcutaneously were connected to EasyMATRIX3 (EMKA Technologies, France). Surface ECGs were recorded in lead I configuration at a frequency of 2 kHz. After 5 min of continuous recording under baseline conditions, the mice received an intravenous injection of atropine (0.5 mg/kg), a muscarinic antagonist, via the jugular vein or an intraperitoneal injection of tertiapin-Q (TPQ; 5 mg/kg), a selective KACh channel blocker.[22] Data were analysed using ECG auto (EMKA Technologies). RR intervals were calculated automatically by a blinded observer from signal-averaged ECG recordings.

2.5 HRV and BRV analysis

Heart rate variability (HRV) and beating rate variability (BRV) were assessed using surface ECG recordings from anaesthetized mice and spontaneous APs from single SAN cells, respectively. HRV and BRV were measured using the square root of the mean of the sum of the squares of successive differences between normal RR intervals (RMSSD, in ms) and the standard deviation of normal RR interval duration (SDNN, in ms).[23,24] RMSSD and SDNN were calculated using the following formulas:

$$ RMSSD = \sqrt{\frac{\sum (NN_n - NN_{n+1})^2}{N}}, $$

$$ SDNN = \sqrt{\frac{\sum (NN_n - \overline{NN})^2}{N - 1}}. $$

2.6 Real-time quantitative PCR

SAN tissues were isolated from NP and P mice and frozen at −80°C until used. For each sample (*n*), three to four SANs were pooled together. Total RNA was isolated using Trizol (Ambion, Life Technologies), treated with DNase I, and then purified with NucleoSpin RNA XS kit (Machery-Nagel, Düren, Germany) according to the manufacturer's instructions. The messenger RNA (mRNA) was measured using a NanoDrop 2000 (Thermo Sientific). Complementary DNA (cDNA) was synthetized with High-capacity cDNA Reverse Transcription Kit (Applied Biosystems, Thermo Fisher Scientific) for 2 h at 37°C using the polymerase chain reaction (PCR) machine PTC-100 Programmable Thermal Controller (MJ Research Inc.). The quantitative PCR (qPCR) reactions were performed with SYBR Select Master Mix (Applied Biosystems) using the real-time PCR QuantStudio3 system (Applied Biosystems). The gene-specific primers used in this study are shown in Supplementary material online, Table S1. All primers were purchased from Integrated DNA Technologies (IDT, Coralville, IA, USA). Both amplification efficacy and gene specificity of the primers were previously validated. qPCR reactions were carried out using a two-step cycle: (i) 15 s at 95°C and (ii) 60 s at 60°C repeated for 40 cycles. Quantitative measurements were performed in duplicate. mRNA expressions from NP and P mice were normalized to three housekeeping genes [hypoxanthine phosphoribosyltransferase (*Hprt*), succinate dehydrogenase subunit A (*Sdha*), and cyclophilin (*Cyclo*)]. Expression data were obtained using $2^{-\Delta\Delta Ct}$ analysis.

2.7 Western blot

SAN protein isolation and western blot protocols were adapted from previous publications.[19,25,26] SAN tissues were isolated from NP and P and frozen at −80°C until use. For each sample (*n*), three SAN were pooled together. SAN tissues were homogenized in a homemade ice-cold extraction buffer containing protease inhibitors (Roche Diagnostics). Triton X-100 (1% final concentration, Bio-Rad) was then added to the extraction buffer, and samples were agitated for 2 h at 4°C. After a 10-min centrifugation at 10 000 *g* at 4°C, the supernatant containing the total protein fraction was collected and stored at −80°C until use. Protein concentrations were assessed using Bradford (Bio-Rad) assay.

Total proteins were heated at 70°C for 90 s, and then 20 μg were loaded and separated on a 4–15% mini-PROTEAN TGX Stain-free precast gel (Bio-Rad, catalogue number: 4568084) (Kir3.1) or a 7.5% hand-cast

polyacrylamide gel (TGX Stain-Free FastCast Acrylamide Kit, Bio-Rad, catalogue number: 1610181) (Kir3.4 and M2R) at 4°C. Activation of the stain-free gel was performed using a ChemiDoc (Bio-Rad, UV light for 45 s). Proteins were then transferred onto a nitrocellulose membrane at 4°C for 90 min at 350 mA. Membrane was blocked at RT in a Tris-buffered saline Tween-20 solution (TBST) containing 1% (Kir3.1/Kir3.4) or 5% (M2R) non-fat dry milk for 1 h and then incubated overnight at 4°C with primary antibody [anti-Kir3.1 (1:500, Alomone APC-005), anti-Kir3.4 (1:1000, Abcam ab219074), anti-M2R (1:500, Alomone AMR-002)]. After three washes of 10 min in TBST/5% non-fat dry milk at RT, membrane was incubated with a goat anti-rabbit (Kir3.1 and M2R) or anti-mouse (Kir3.4) horseradish peroxidase–conjugated secondary antibody (1:10 000) for 1 h. Finally, after three 10-min washes in TBST, the membrane was soaked for ~1 min in Western Lightning Plus-ECL (PerkinElmer). Bands of interest were detected and visualized with a ChemiDoc. Using Image Lab software, Kir3.1, Kir3.4, and M2R expression was normalized to the total protein revealed by stain-free quantification.

2.8 Drugs

CCh and atropine were both purchased from Sigma-Aldrich (Milwaukee, WI, USA) and first dissolved in distilled water as a stock solution (10 mM). TPQ was purchased from Alomone (Jerusalem, Israel) and first dissolved in distilled water as a stock solution of 306 µM. To achieve their respective final concentration, stock solution of CCh was diluted in Tyrode's solution, while stock solution of atropine and TPQ was diluted in saline (0.9% NaCl).

2.9 Statistical analysis

Results are reported as mean ± standard error of mean, where 'n' represents the number of cells and 'N' the number of mice. Unpaired Student t-test was used to compare cellular electrophysiology, gene/protein expression, and ECG data between two different groups. Paired Student t-test was used to compare the same animal/cell before and after drug administration. Two-way analysis of variance (ANOVA) was used to compare current-voltage (IV) curves between the two groups. Results were considered statistically significant when $P < 0.05$. All statistical analyses were performed with GraphPad Prism.

3. Results

3.1 I$_{KACh}$ current density is decreased in SAN cells from P mice

We first compared I$_{KACh}$ current density in SAN cells from NP and P mice to determine whether a reduction in I$_{KACh}$ density depolarizes the MDP of SAN AP, leading to accelerated cardiac automaticity during pregnancy. Whole-cell voltage-clamp techniques were used to record I$_{KACh}$ and CCh superfusion was applied to activate I$_{KACh}$.[27] Supplementary material online, Figure S1 shows that maximal activation of I$_{KACh}$ was obtained with 10 µM of CCh. Currents recorded under control conditions were subtracted from those in the presence of CCh to obtain the CCh-sensitive current shown in Supplementary material online, Figure S2A, using a ramp protocol (left) and a voltage-step protocol (right). The data presented in Supplementary material online, Figure S2A and B first confirm that the ramp and step protocols can be used for these experiments. As both voltage protocols yield similar current–voltage (IV) relationships, the ramp protocol was used throughout the study for I$_{KACh}$ recording. Supplementary material online, Figure S2C shows that the increase in I$_{KACh}$ current after application of 10 µM of CCh returned to control values after CCh washout.

Using the voltage ramp protocol and the superfusion of 10 µM of CCh as described above, we then compared I$_{KACh}$ current density in SAN cells from NP and P mice. As shown in the representative current recordings in Figure 1A, I$_{KACh}$ was greatly reduced in P mice compared with NP mice. This is also illustrated in the mean IV curves, showing a much lower density

of I$_{KACh}$ in SAN cells from P mice (Figure 1B). For instance, the bar graph in Figure 1C shows a 46% reduction in I$_{KACh}$ density at −55 mV, a voltage close to the MDP, where I$_{KACh}$ plays a critical role.

3.2 SAN expression of the acetylcholine-activated K$^+$ channel is reduced during pregnancy

Next, to explain the lower density of I$_{KACh}$ in P mice, we used real-time qPCR to measure and compare the SAN mRNA level of genes involved in I$_{KACh}$ function in NP and P mice (Figure 2A). Specifically, we examined the genes underlying Kir3.1/GIRK1 (Kcnj3), Kir3.4/GIRK4 (Kcnj5), the muscarinic receptor M2R (Chrm2), the adenosine receptor A1R (Adora1), and the two regulators of G protein signalling 4 and 6 (Rgs4 and Rgs6), normally required for the attenuation of parasympathetic-dependent G protein signalling in the SAN (Figure 2B). Of these, only Kcnj3 was decreased by 26% in SAN during pregnancy. Western blot analysis revealed a corresponding decrease in Kir3.1 protein levels in the SAN during pregnancy (Figure 2C). There was a trend towards reduced Kir3.4 protein expression in the SANs of P mice, which was not statistically significant. M2R protein expression was reduced by ~30% during pregnancy, although Chrm2 mRNA was not altered. Stain-free membranes used to normalize protein expression are available in Supplementary material online, Figure S3. Overall, these expression studies are consistent with the lower density of I$_{KACh}$ and demonstrate that pregnancy results in a decrease in Kcnj3/Kir3.1 and M2R.

## 3.3 SAN APs are less sensitive to CCh during pregnancy

To gain insight on the functional effect of I$_{KACh}$ reduction in P mice, we next examined the impact of CCh on spontaneous APs of SAN cells in NP and P mice. Figure 3A shows typical spontaneous APs recorded before (left) and after (right) superfusion of 0.1 µM of CCh in a NP mouse. As illustrated, the AP rate was reduced in the presence of CCh, without hyperpolarization of the MDP, suggesting that I$_{KACh}$ was unaffected at low concentration of CCh. The data reported in Figure 3B confirmed that 0.1–0.5 µM of CCh had no effect on MDP. We have previously shown that the response of I$_f$ to muscarinic stimulation was similar in SAN cells from NP and P mice.[6] The decrease in AP rate observed in the present study is therefore likely due to the effects of CCh on other ionic conductances, such as I$_{CaL}$ and Ca^{2+} cycle mechanisms, also involved in the diastolic depolarization (DD) phase of the SAN AP.[28] However, when cells were exposed to 1 µM of CCh, a concentration shown to activate I$_{KACh}$, a significant hyperpolarization of the MDP was observed (Figure 3B and C), which caused the AP to stop firing. However, once the CCh was removed, the SAN AP firing rate returned to normal. Importantly, when the same experiments were performed on P mice, CCh-induced MDP hyperpolarization was much weaker, consistent with the lower I$_{KACh}$ density in pregnancy (Figure 3D).

3.4 HR response to atropine and TPQ is altered during pregnancy

The effects of atropine, a potent M2R antagonist, were then studied to determine whether HR during pregnancy responded differently to muscarinic modulation. Figure 4A shows representative surface ECG traces comparing HR in NP and P mice before and after atropine administration (0.5 mg/kg). The bar graphs reported in Figure 4B show the mean data obtained for both groups during these experiments, with the right-hand panel showing the mean change in HR obtained by averaging the differences between individual mice before and after atropine administration. Atropine increased HR in NP mice by 14% (ΔHR: 66 ± 8 bpm) but had no significant effect on P mice.

Additional ECG recordings were obtained in the presence of TPQ (5 mg/kg), a selective blocker of KACh channels (Figure 4C). As shown in Figure 4D, the increase in HR produced by TPQ was much more pronounced in NP mice (13%; ΔHR: 62 ± 8 bpm) than in P mice (2%; ΔHR:
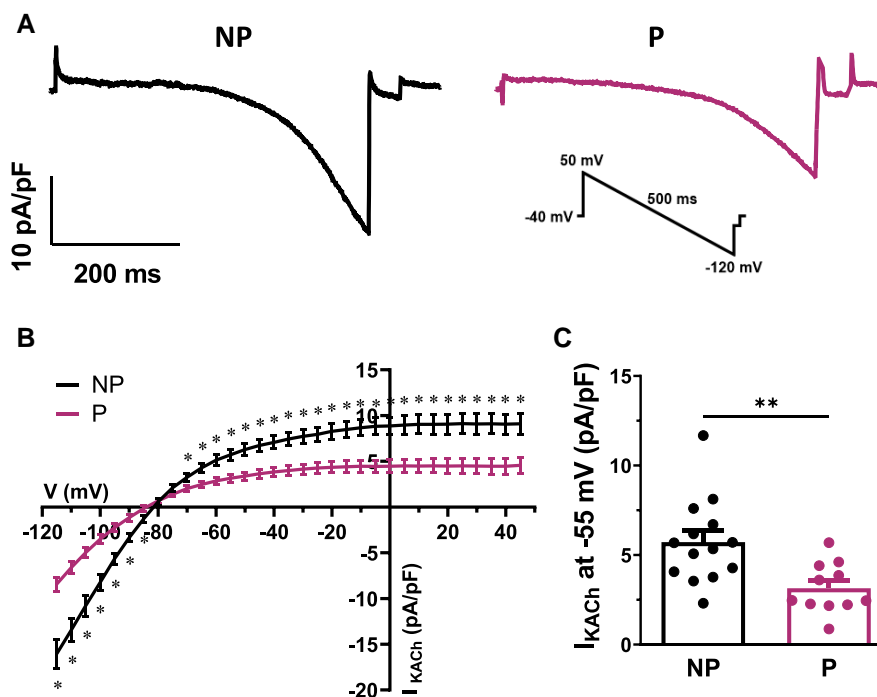
Figure 1 Pregnancy decreases the density of the acetylcholine-activated K$^+$ current (I_{KACh}) in mouse SAN cells. (*A*) Typical I_{KACh} recordings in NP and P mice obtained with the ramp protocol shown in inset. (*B*) Mean IV relationships show a significantly lower I_{KACh} density in SAN cells from P mice compared with NP mice [NP (*n* = 14, *N* = 10) vs. P (*n* = 11, *N* = 5): *P < 0.05 from −115 to −85 mV and from −70 to +45 mV]. (*C*) At −55 mV, mean I_{KACh} density is decreased in P mice (3.1 ± 0.4 pA/pF) compared wth NP mice (5.7 ± 0.6 pA/pF, P = 0.0026). Two-way ANOVA was used.

12 ± 4 bpm). This reduced sensitivity of HR to atropine and TPQ during pregnancy is consistent with the lower density of I_{KACh}.

3.5 HRV and SAN BRV are altered during pregnancy

Not only does I_{KACh} play an essential role in controlling SAN pacemaker activity, but previous studies have also shown that a decrease in I_{KACh} density leads to a reduction in HRV.[29–31] Therefore, in the next series of experiments, HRV and BRV were measured to provide further evidence of the functional role of I_{KACh} during pregnancy. First, we compared HRV between NP and P mice using surface ECG data obtained from anaesthetized mice. Consistent with our previous work, we found that RR intervals were reduced by 15% during pregnancy in mice (*Figure 5A* and *B*). In addition, RMSSD and SDNN, which were used to analyse HRV, were also reduced in P mice (*Figure 5B*), indicating lower fluctuations in HRV during pregnancy. It should be noted that a reduction in HRV has been associated with negative cardiovascular outcomes.[32,33] Additionally, data reported in *Figure 5C* and *E* show that RMSSD was reduced in NP mice by 56 and 57% after atropine and TPQ administration, respectively, whereas RMSSD in P mice was unaffected by either drug. Similar observations were observed in both groups for SDNN (*Figure 5D* and *F*). Overall, these results support a role of I_{KACh} in regulating HR changes during pregnancy.

Furthermore, the data reported in *Figure 5C* and *E* show that RMSSD was reduced in NP mice by 56 and 57% after administration of atropine and TPQ, respectively, whereas RMSSD in P mice was unaffected by either drug. Similar observations were made in both groups for RMSSD (*Figure 5D* and *F*).

Similar results were also observed at cellular level when HRV analysis was complemented by a comparison of beat-to-beat variability between SAN cells from NP and P mice (*Figure 5G* and *H*). As illustrated in

Figure 5G and *H*, the firing rate of the spontaneous AP of the SAN cells was higher in P mice compared with NP mice, with a 15% reduction in inter-beat intervals, in line with their increased HR. This was associated with a lower RMSSD and SDNN (*Figure 5H*). Collectively, these results confirm that lower I_{KACh} channel activity is associated with reduced HRV and alteration in HR modulation by the parasympathetic nervous system during pregnancy.

3.6 Reduction of I_{KACh} density is reversed after delivery

In women, the increase in HR associated with pregnancy is reversed within 14 days of delivery.[34] We have previously shown that the same phenomenon also occurs in mice, where HR returns to control values at early post-partum (PP),[7] i.e. 24–48 h after delivery. So, to determine whether the changes observed in I_{KACh} follow the same pattern, PP mice were included in this study. The results summarized in *Figure 6* compare I_{KACh} current density in SAN cells from NP and PP mice. As shown by typical I_{KACh} current recordings (*Figure 6A*) and its mean IV curves (*Figure 6B*), I_{KACh} current density was identical between the two groups (*Figure 6B* and *C*). These data clearly indicate that the effect of pregnancy on I_{KACh} is reversible shortly after delivery.

4. Discussion

4.1 Summary of main findings

This study describes the contribution of I_{KACh} to the positive chronotropic effects of pregnancy. KACh is an inward rectifying potassium channel strongly expressed in the SAN and consists of Kir3.1 and Kir3.4 channel subunits, both of which are required to have a functional I_{KACh} current.
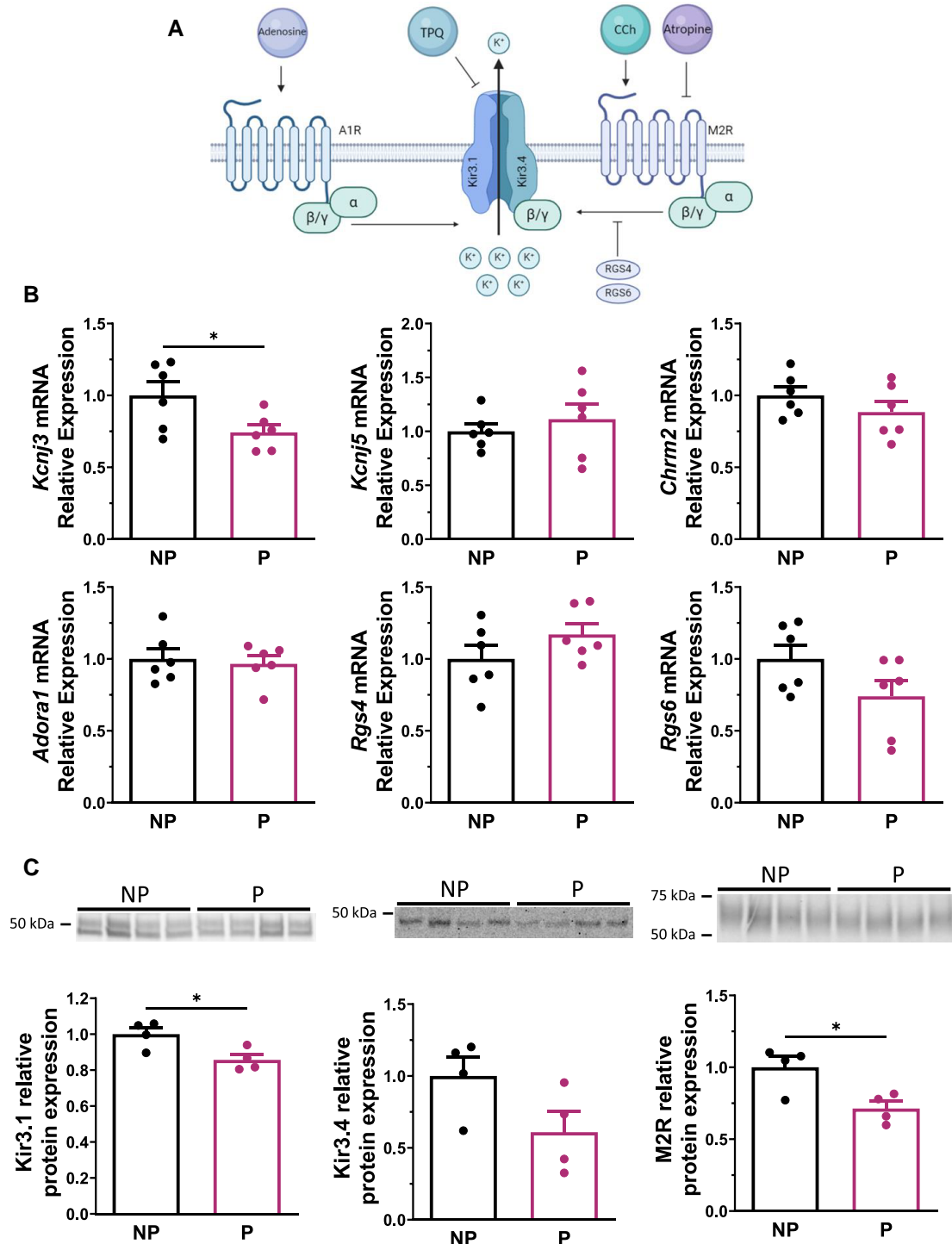
Figure 2 Kir3.1 and M2R expressions are decreased during pregnancy in mouse SAN tissue. (*A*) Mechanism of I_KACh in SAN cell. When CCh binds the M2R, the Gβγ complex binds the heterotetrameric channel composed of both Kir3.1 and Kir3.4, which generates I_KACh. RGS4 and RGS6, two regulators of G protein signalling in SAN tissue, are known to prevent the binding of Gβγ to the Kir channel and inhibit I_KACh. The G protein of the adenosine a1 receptor (A1R) is also known to activate the channel composed of Kir3.1 and Kir3.4. TPQ is a selective KACh channel blocker. (*B*) qPCR data showing mRNA relative expression of *Kcnj3* (Kir3.1/GIRK1; $P = 0.037$), *Kcnj5* (Kir3.4/GIRK4; $P = 0.493$), *Chrm2* (M2R; $P = 0.262$), *Adora1* (A1R; $P = 0.713$), *Rgs4* (RGS4; $P = 0.193$), and *Rgs6* (RGS6; $P = 0.110$) from NP and P mice ($N = 6$/group). Only *Kcnj3* is decreased in P mice compared with NP mice (NP: 1.00 ± 0.09; P: 0.74 ± 0.05). (*C*) Western blot of Kir3.1 (left), Kir3.4 (middle), and M2R (right) protein in NP and P mice ($N = 4$/group). Densitometry analysis shows a reduction of Kir3.1 (NP: 1.00 ± 0.04; P: 0.86 ± 0.03, $P = 0.024$) and M2R (NP: 1.00 ± 0.08; P: 0.71 ± 0.05, $P = 0.021$) expression during pregnancy, although Kir3.4 is not statistically different between the two groups (NP: 1.00 ± 0.13; P: 0.61 ± 0.14, $P = 0.094$). Total protein content on stain-free was used to normalize protein signal (see Supplementary material online, *Figure S3*). Unpaired Student *t*-test was used in all figures unless specified otherwise.
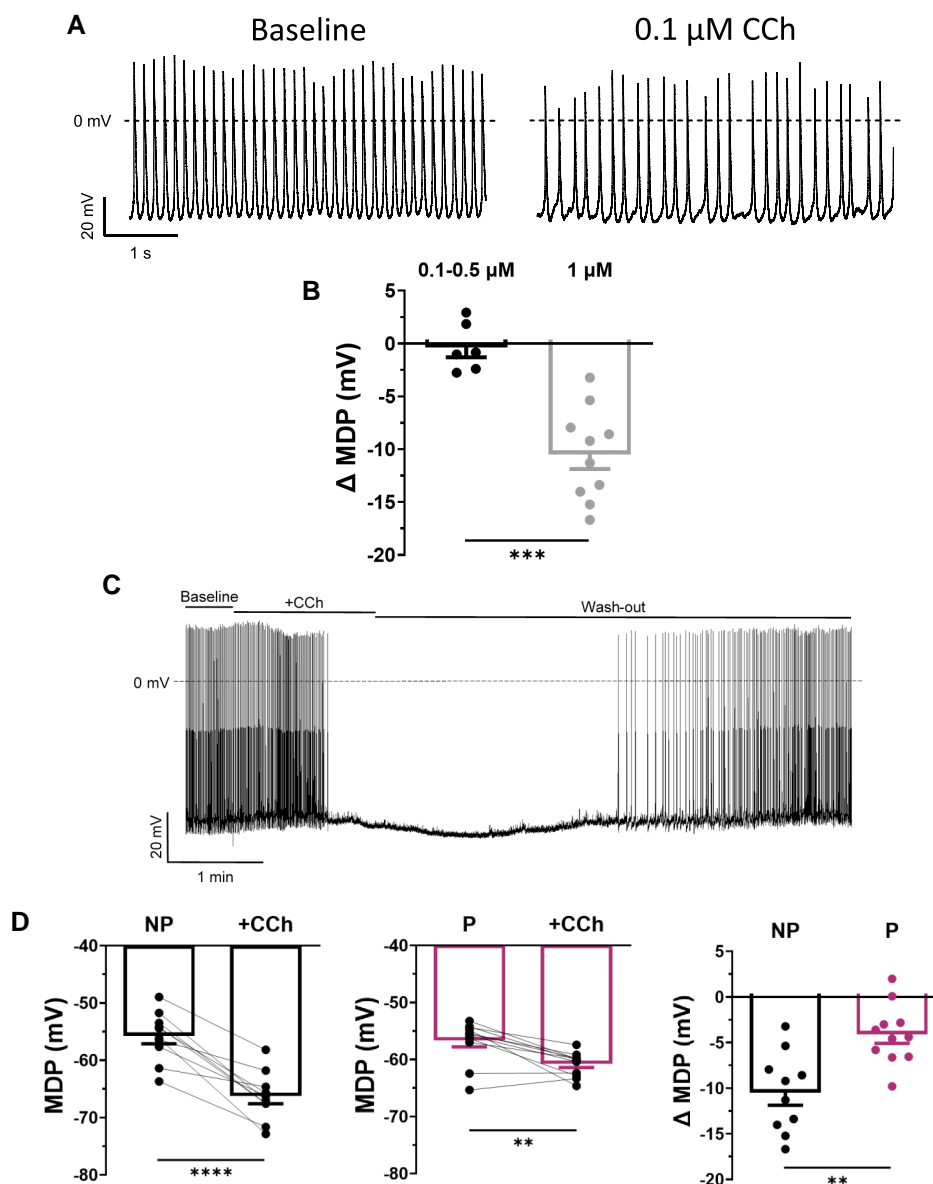
Figure 3 The CCh sensitivity of SAN cells is reduced during pregnancy. (*A*) Typical recordings of spontaneous AP of SAN cells from NP mice in baseline condition and after application of 0.1 μM of CCh. (*B*) Bar graph shows that MDP is not altered by the application of 0.1–0.5 μM CCh (ΔMDP: −0.4 ± 0.9 mV; $n = 6$, $N = 3$) and is hyperpolarized after the application of 1 μM of CCh (ΔMDP: −10.5 ± 1.4 mV; $n = 10$, $N = 6$, $P = 0.00014$). (ΔMDP compared with respective controls, NP vs. NP + 0.1–0.5 μM CCh, $P = 0.708$; NP vs. NP + 1 μM CCh, $P = 0.00003$, *paired Student *t*-test). (*C*) Typical example of continuous recordings of spontaneous APs of SAN cells from NP mice under baseline conditions, in the presence of CCh (1 μM), and washout. (*D*) Application of CCh hyperpolarizes the MDP of spontaneous AP of both (left) NP (−55.8 ± 1.4 mV, +CCh: −66.3 ± 1.4 mV; $n = 10$, $N = 6$, $P = 0.00003$) and (middle) P (−56.8 ± 1.1 mV, +CCh: −60.9 ± 0.6 mV; $n = 11$, $N = 4$, $P = 0.0019$) mice. Paired Student *t*-test was used. (right) Bar graph shows the ΔMDP of NP and P SAN cells. The MDP is significantly less sensitive to CCh during pregnancy (ΔMDP: NP: −10.5 ± 1.4 mV, P: −4.1 ± 1.0 mV; $P = 0.0012$).

We first compared the expression and functional role of I_{KACh} in SAN from NP and P mice. We found a significant decrease in I_{KACh} density in SAN cells from P mice, associated with a decrease in *Kcnj3*/Kir3.1 and M2R expression. Using SAN AP recordings and surface ECG data, we then found altered responsiveness to muscarinic manipulation in P mice. Furthermore, the effect on HR observed with TPQ, a selective KACh blocker, confirms reduced I_{KACh} function during pregnancy. Interestingly, changes in I_{KACh} were reversible in PP mice, as was the pregnancy-induced

increase in HR.[7] Overall, these observations suggest that the reduction in I_{KACh} also contributes to the increase in HR associated with pregnancy.

4.2 Relationship with previous findings

Although the incidence of cardiac arrhythmias is increasing during pregnancy,[5] the underlying mechanisms remain largely unexplored. To our knowledge, our group is the only one to have studied the electrical
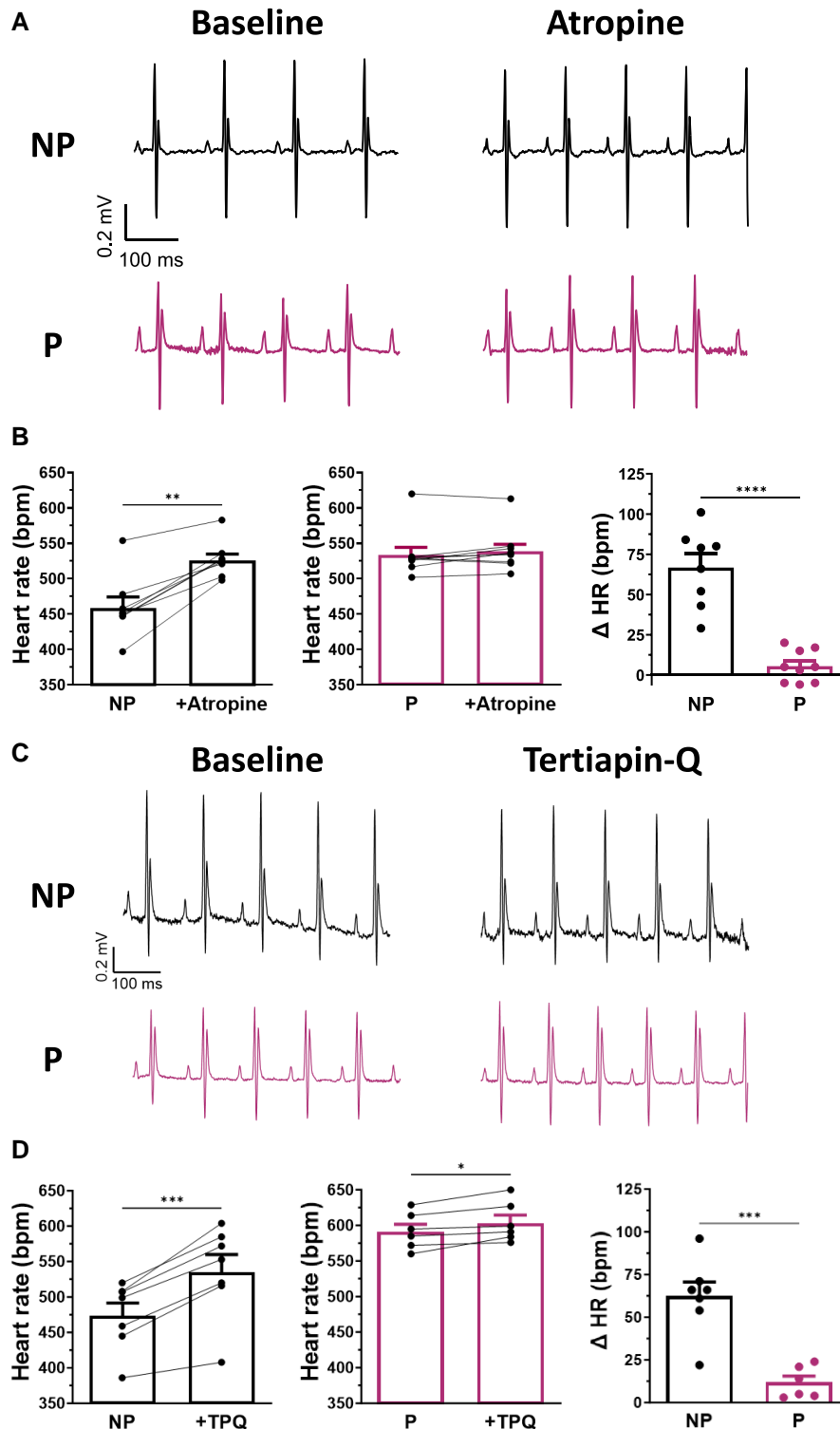
Figure 4 Pregnancy modifies the HR response to parasympathetic antagonist atropine. (*A*) Typical ECG recordings in NP (upper panel) and P (lower panel) mice before (baseline, left) and after (right) intravenous injection of atropine solution (0.5 mg/kg). (*B*) Atropine (left) increased HR of NP mice (461 ± 17 bpm, +Atropine: 527 ± 10 bpm, *N* = 8, *P* < 0.0001), (middle) whereas atropine has no effect on HR of P mice (535 ± 12 bpm, +atropine: 540 ± 11 bpm, *N* = 9, *P* = 0.145). Paired Student *t*-test was used. (right) Bar graph reports the ΔHR of NP and P mice after atropine administration. HR is significantly more responsive to atropine in NP compared with P mice (ΔHR: NP: 66 ± 8 bpm; P: 5 ± 3 bpm, *P* < 0.0001). (*C*) Typical ECG recordings in NP (upper panel) and P (lower panel) mice before (baseline, left) and after (right) intra-peritoneal injection of TPQ (5 mg/kg). (*D*) (left) TPQ increased HR in NP mice (475 ± 18 bpm, +TPQ: 537 ± 25 bpm, *N* = 7, *P* = 0.0003) and, to a much lesser extent, HR in P mice (593 ± 11 bpm, +TPQ: 605 ± 12 bpm, *N* = 6, *P* = 0.024). Paired Student *t*-test was used. (*right*) The bar graph shows the ΔHR of NP and P mice after TPQ administration. HR is significantly more sensitive to TPQ in NP than in P mice (ΔHR: NP: 62 ± 8 bpm; P: 12 ± 4 bpm, *P* = 0.0003).
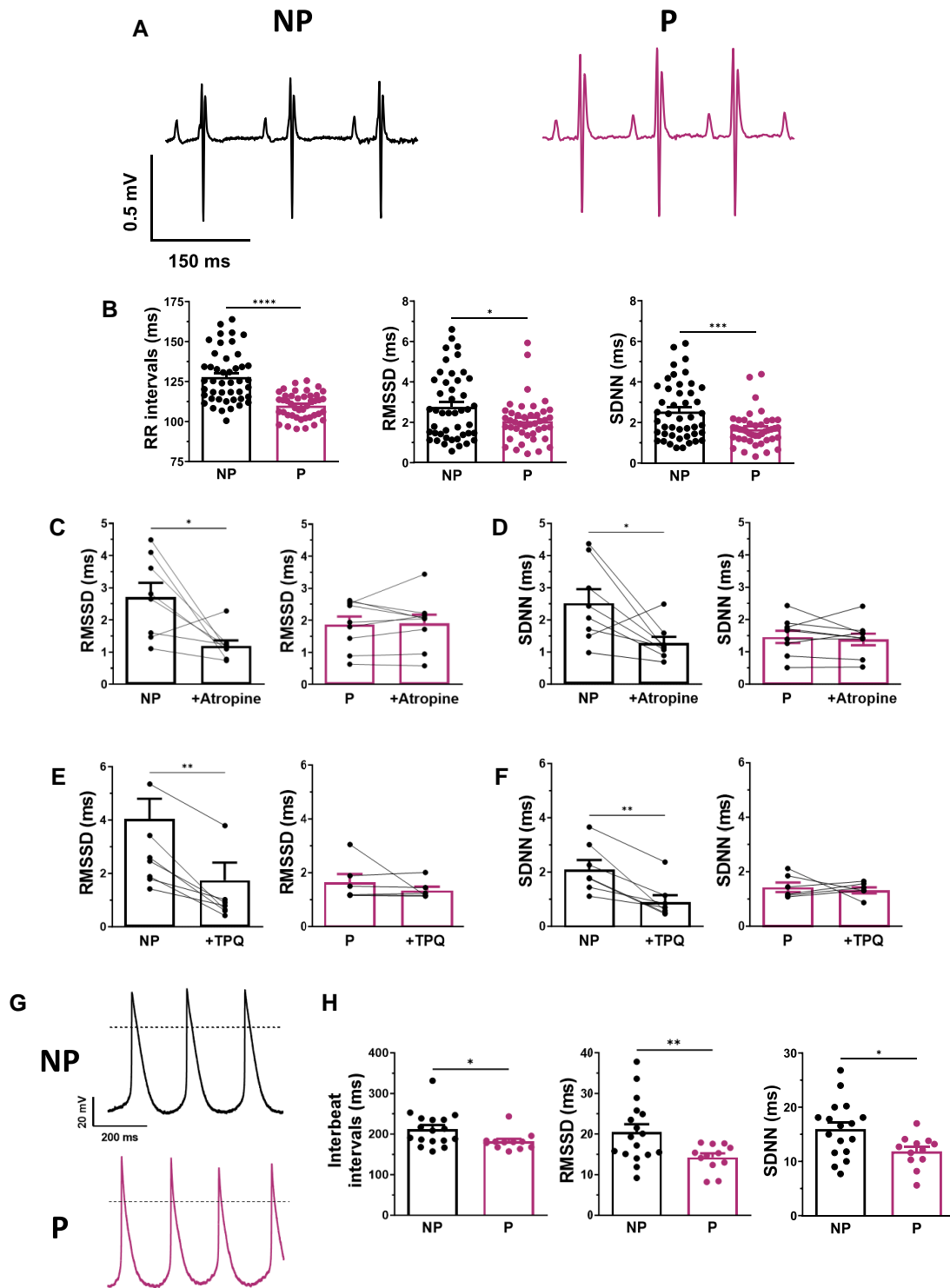
Figure 5 HRV and BRV are both reduced in pregnancy. (*A*) Typical surface ECG recordings in anaesthetized NP and P mice. *In vivo*, pregnancy reduces (*B*) (left) RR intervals (NP: 128 ± 2 ms, N = 45; P: 110 ± 1 ms, N = 43, P < 0.00001), (middle) RMSSD (NP: 2.76 ± 0.25 ms; P: 2.06 ± 0.16 ms, P = 0.0186), and (right) SDNN (NP: 2.54 ± 0.21 ms; P: 1.67 ± 0.13 ms, P = 0.00066). (*C, D*) Atropine (left) decreased RMSSD (2.73 ± 0.48 ms, +atropine: 1.21 ± 0.18 ms, P = 0.023) and SDNN (2.53 ± 0.47 ms, +atropine: 1.28 ± 0.21 ms, P = 0.033) in NP mice (N = 8) but (right) has no effect on RMSSD (1.88 ± 0.27 ms, +atropine: 1.91 ± 0.29 ms, P = 0.818) nor SDNN (1.50 ± 0.20 ms, +atropine: 1.41 ± 0.19 ms, P = 0.571) in P mice (N = 9). Paired Student *t*-test was used. (*E, F*) TPQ (left) decreased RMSSD (2.70 ± 0.51 ms, +TPQ: 1.17 ± 0.44 ms, P = 0.0014) and SDNN (2.15 ± 0.34 ms, +TPQ: 0.94 ± 0.25 ms, P = 0.0027) in NP mice (N = 7) but (right) has no effect on RMSSD (1.66 ± 0.30 ms, +TPQ: 1.36 ± 0.14 ms, P = 0.392) nor SDNN (1.46 ± 0.18 ms, +TPQ: 1.35 ± 0.11 ms, P = 0.694) in P mice (N = 6). Paired Student *t*-test was used. (*G*) Typical spontaneous AP recordings of SAN cells from NP and P mice. (*H*) At cellular level, there is a decrease in (left) inter-beat intervals (NP: 212 ± 10 ms, n = 17, N = 10; P: 182 ± 6 ms, n = 12, N = 10, P = 0.020), (middle) RMSSD (NP: 20.5 ± 1.9 ms; P: 14.3 ± 1.0 ms, P = 0.0071), and (right) SDNN (NP: 16.0 ± 1.3 ms; P: 11.9 ± 0.9 ms, P = 0.020).
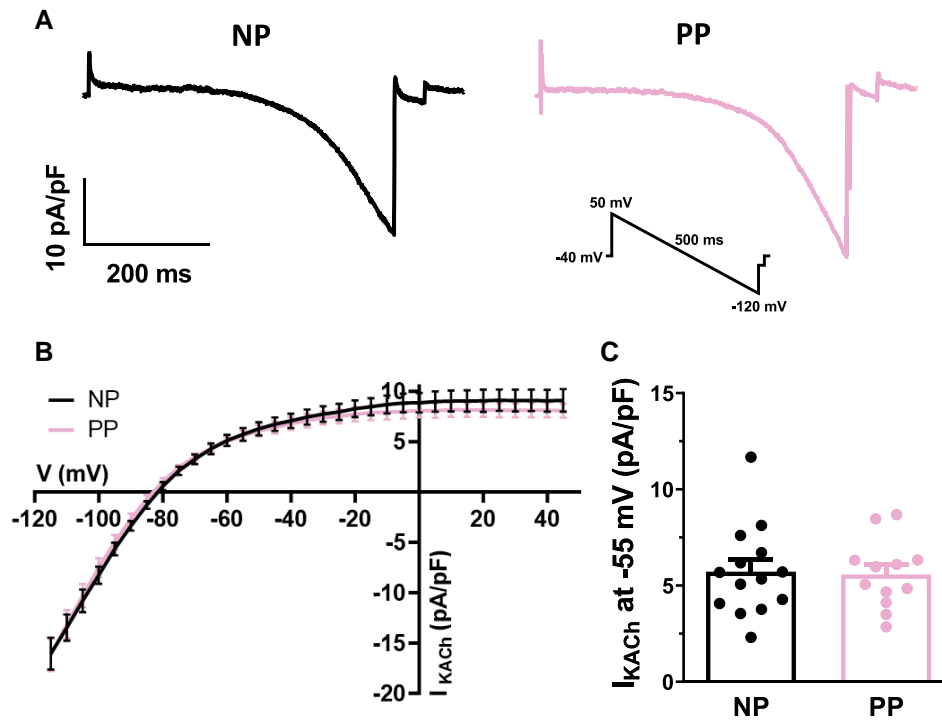
Figure 6 Reduction of I_KACh density is reversed following delivery. (A) Typical example of I_KACh recordings obtained in NP and PP mice. Inset shows ramp protocol. (B) Mean IV curves show nearly identical current of I_KACh density in SAN cells from NP ($n = 14$, $N = 10$) and PP ($n = 12$, $N = 6$) mice ($P > 0.05$). (C) Mean I_KACh current at -55 mV is similar in both NP and PP mice (NP: 5.7 ± 0.6 pA/pF; PP: 5.6 ± 0.5 pA/pF; $P = 0.8639$). Two-way ANOVA was used.

remodelling of the SAN during pregnancy using a murine model of pregnancy. Thus far, we have identified some of the mechanisms contributing to the positive chronotropic effects of pregnancy. Our initial study showed that P mice reproduce the increased HR observed in human pregnancy.[6] We also found that pregnancy induces an important up-regulation of the pacemaker current I_f in mouse SAN and contributes to faster automaticity.[6] We then confirmed that, like women, P mice not only have a higher HR but are also more vulnerable to supraventricular tachyarrhythmias.[7] We also reported that, in addition to changes in I_f current, other mechanisms were involved. Specifically, we demonstrated a major role for changes in calcium homoeostasis.[7] We also reported that HR in P mice returns to control values soon after delivery.[7] This rapid reversal of the electrophysiological and calcium homoeostasis changes to baseline levels argues for a hormonal effect on ion channels during pregnancy. Based on these observations, we then provided strong evidence showing that 17β-oestradiol, at levels found in late pregnancy, recapitulated the increased HR and accelerated SAN automaticity observed in pregnancy by regulation of I_f through the oestrogen receptor α.[11]

In this study, we wanted to test whether a reduction in I_KACh could also contribute to the elevated HR associated with pregnancy. In the SAN, I_KACh plays an important role in HR as it is known to have a negative chronotropic effect on the regulation of the cardiac pacemaking activity.[10] Indeed, this repolarizing current predominates around the DD of the SAN AP and its activation hyperpolarizes the MDP, slowing down the DD rate and consequently HR.[14,30] Here, we showed that SAN from P mice exhibited a reduced Kir3.1 and M2R protein expression, and I_KACh density, decreasing the responsiveness of the SAN following cholinergic stimulation and reducing its impact on the MDP. This could contribute to the pregnancy-induced accelerated HR. Consistent with our findings, previous studies have reported similar results using a Kir3.4 knockout mouse model. The absence of functional I_KACh impaired

the muscarinic response of the SAN, resulting in increased HR.[29,30] Furthermore, it has also been shown in humans that a gain of function of Kir3.4 causes sinus node dysfunction, due to increased I_KACh density and hyperpolarization of the SAN AP.[35] Taken together, the results of these previous reports and those of the present study strongly support an important role for I_KACh in the mechanisms of SAN automaticity and arrhythmia.[22,36]

I_KACh and HRV are closely related. Indeed, HRV can be regulated by the autonomic nervous system, as well as the intrinsic SAN activity. Since I_KACh is activated by acetylcholine, a parasympathetic neurotransmitter, and its channel is an integral part of the SAN, BRV and HRV were measured on spontaneous AP and surface ECG recordings, respectively. Here, we showed that pregnancy is associated with a lower HRV in mice, at both cellular level and in vivo. These results are in line with clinical findings, as P women also show a reduction in HRV.[37] A high HRV generally corresponds to good cardiac health[32] and indicates that the HR can adjust and recover from a stress and/or a stimulation.[23] Conversely, a low HRV is predictive of negative cardiovascular outcomes, as the beat-to-beat variation of the HR is less adaptable.[23] Thus, the lower HRV observed in pregnancy can affect cardiac adaptation and lead to maternal complications,[38] including supraventricular arrhythmias[39] observed in both P women and mice. Analysis of BRV in isolated SAN myocytes is valuable because it allows us to determine that changes in HRV are due, at least in part, to intrinsic changes in SAN function. Explicitly, our study highlights an association between changes in HRV and I_KACh during pregnancy. In further support of a relationship between I_KACh and HRV, previous studies have shown that alterations in key proteins involved in I_KACh activation, such as ion channel α-subunits and their regulators, also affect HRV. For example, Wickman et al.[29] showed reduced HRV in a Kir3.4 knockout mouse model. Similarly, another group reported that loss of Rgs6, which negatively regulated I_KACh in SAN, increased HRV.[31] In agreement with these studies, we

found that reduced Kir3.1 mRNA and protein expression in SAN was associated with lower HRV during pregnancy.

The changes in I_{KACh} were fully reversible shortly after delivery, which is consistent with our previous data showing that HR in P mice also returns to control values in early PP.[7] The I_{KACh} data are also consistent with our previous work where we identified other ionic mechanisms contributing to pregnancy-induced positive chronotropic effects[6,7] that also rapidly return to baseline levels in PP mice.[7] Equally important, the same phenomenon is also observed in women, where HR has been shown to return to pre-pregnancy values within 2 weeks after delivery.[2,34] This further underlines the dynamic nature of the SAN, which must be highly adaptable to meet the increased physiological demands of pregnancy.[1,40]

In this and previous studies, our group has explored the electrical remodelling of the SAN responsible for accelerated HR in pregnancy.[6,7,11,12] Although necessary to meet the increased physiological demand associated with pregnancy, this elevated HR may lead to supraventricular arrhythmias.[8] It is worth mentioning that our results were obtained in young, healthy female mice undergoing their first gestation. It is therefore highly conceivable that the SAN would respond differently to gestation at a later age, in the presence of maternal complications, or during subsequent pregnancies. These conditions could lead to poor adaptation of the SAN and further increase the risk of pregnancy-induced arrhythmias.

4.3 Limitations

We demonstrated that the response to TPQ, a specific blocker of I_{KACh}, was reduced in P mice, confirming the role of I_{KACh} in pregnancy-induced increased HR. However, we did not provide cellular electrophysiological data to further differentiate whether Kir3.1 or Kir3.4 subunits are selectively affected. To achieve this, specific blockers for these subunits would be necessary. However, it is important to note that KACh is a heterotetrameric channel composed of both Kir3.1 and Kir3.4 subunits, and both are essential for its functional current. Consequently, reducing only one subunit, here Kir3.1, would lead to a decreased I_{KACh} current density. Additionally, our western blot data indicate that only Kir3.1 protein expression is significantly decreased in the SAN of P mice, reinforcing our conclusion that the observed effects are mediated by changes in Kir3.1 rather than Kir3.4. Although the study provides valuable insights into the intrinsic mechanisms affecting HR in P mice and highlights the reduced expression of Kir3.1 and M2R in the SAN as a contributing factor, it should be noted that no direct assessment of parasympathetic nerve activity in P mice has been conducted. It would be useful to explore this aspect in future studies, as they could provide further insights into the complexities of HR control during pregnancy.

5. Conclusion

In this study, we demonstrate that, in addition to the already documented electrical remodelling of the SAN,[6,7,11,12] important functional changes in I_{KACh} also contribute to increased SAN automaticity and elevated HR during pregnancy. Ultimately, a better understanding of the mechanisms underlying SAN electrical remodelling during pregnancy could lead to improved management of pregnancy-related cardiac arrhythmias. This becomes all the more crucial as the incidence of cardiac arrhythmias is rising, partly due to increasing maternal age and age-related comorbidities.[41]

Translational perspective

Pregnant women have a higher incidence of cardiac arrhythmias. Pregnancy is also associated with elevated resting heart rate, a known risk factor for arrhythmias, suggesting an influence on sinoatrial node automaticity. As the incidence of pregnancy-related arrhythmias is now rising, understanding the underlying mechanisms is increasingly important. Using a pregnancy mouse model, we demonstrated that a reduction in the acetylcholine-activated potassium current, I_{KACh}, in sinoatrial node plays a critical role in pregnancy-related accelerated heart rate. This work addresses an important topic in women's health as it provides novel and functional insight into the mechanisms in pregnancy-induced cardiac arrhythmias.

Supplementary material

Supplementary material is available at *Cardiovascular Research* online.

Authors' contributions

All experiments were performed in Dr Céline Fiset's Laboratory. V.L. conducted all experiments, analysed the data, generated the figures/tables, and drafted the manuscript. G.E.G. generated the initial ECG observations and helped conceptualize the ECG study. E.L. and M.S. performed western blots and helped with ECG analysis. C.F. studied the conceptualization, manuscript drafting, and final version. All authors approved the final version of the manuscript.

References

1. Sanghavi M, Rutherford JD. Cardiovascular physiology of pregnancy. *Circulation* 2014;**130**: 1003–1008.
2. Hunter S, Robson SC. Adaptation of the maternal heart in pregnancy. *Br Heart J* 1992;**68**: 540–543.
3. Enriquez AD, Economy KE, Tedrow UB. Contemporary management of arrhythmias during pregnancy. *Circ Arrhythm Electrophysiol* 2014;**7**:961–967.
4. Safavi-Naeini P, Sorurbakhsh NZ, Razavi M. Cardiac arrhythmias during pregnancy. *Tex Heart Inst J* 2021;**48**:e217548.
5. Tamirisa KP, Elkayam U, Briller JE, Mason PK, Pillarisetti J, Merchant FM, Patel H, Lakkireddy DR, Russo AM, Volgman AS, Vaseghi M. Arrhythmias in pregnancy. *JACC Clin Electrophysiol* 2022;**8**:120–135.
6. El Khoury N, Mathieu S, Marger L, Ross J, El Gebeily G, Ethier N, Fiset C. Upregulation of the hyperpolarization-activated current increases pacemaker activity of the sinoatrial node and heart rate during pregnancy in mice. *Circulation* 2013;**127**:2009–2020.
7. El Khoury N, Ross JL, Long V, Thibault S, Ethier N, Fiset C. Pregnancy and oestrogen regulate sinoatrial node calcium homeostasis and accelerate pacemaking. *Cardiovasc Res* 2018;**114**: 1605–1616.
8. Burkart TA, Conti JB. Cardiac arrhythmias during pregnancy. *Curr Treat Options Cardiovasc Med* 2010;**12**:457–471.
9. Choudhury M, Boyett MR, Morris GM. Biology of the sinus node and its disease. *Arrhythm Electrophysiol Rev* 2015;**4**:28–34.
10. Mangoni ME, Nargeot J. Genesis and regulation of the heart automaticity. *Physiol Rev* 2008; **88**:919–982.

11. Long V, Fiset C. Contribution of estrogen to the pregnancy-induced increase in cardiac automaticity. *J Mol Cell Cardiol* 2020;**147**:27–34.

12. Long V, Mathieu S, Fiset C. Pregnancy-induced increased heart rate is independent of thyroid hormones. *Heart Rhythm O2* 2021;**2**:168–173.

13. Aziz Q, Li Y, Tinker A. Potassium channels in the sinoatrial node and their role in heart rate control. *Channels (Austin)* 2018;**12**:356–366.

14. MacDonald EA, Rose RA, Quinn TA. Neurohumoral control of sinoatrial node activity and heart rate: insight from experimental models and findings from humans. *Front Physiol* 2020;**11**:170.

15. Wickman K, Krapivinsky G, Corey S, Kennedy M, Nemec J, Medina I, Clapham DE. Structure, G protein activation, and functional relevance of the cardiac G protein-gated K$^+$ channel, IKACh. *Ann N Y Acad Sci* 1999;**868**:386–398.

16. Cifelli C, Rose RA, Zhang H, Voigtlaender-Bolz J, Bolz S-S, Backx PH, Heximer SP. RGS4 regulates parasympathetic signaling and heart rate control in the sinoatrial node. *Circ Res* 2008;**103**:527–535.

17. Kulkarni K, Xie X, Fernandez de Velasco EM, Anderson A, Martemyanov KA, Wickman K, Tolkacheva EG. The influences of the M2R-GIRK4-RGS6 dependent parasympathetic pathway on electrophysiological properties of the mouse heart. *PLoS One* 2018;**13**:e0193798.

18. McLendon K, Preuss CV. *Atropine*. Treasure Island (FL): StatPearls Publishing; 2023.

19. Liu Y, Jansen HJ, Krishnaswamy PS, Bogachev O, Rose RA. Impaired regulation of heart rate and sinoatrial node function by the parasympathetic nervous system in type 2 diabetic mice. *Sci Rep* 2021;**11**:12465.

20. Verkerk AO, Geuzebroek GSC, Veldkamp MW, Wilders R. Effects of acetylcholine and noradrenalin on action potentials of isolated rabbit sinoatrial and atrial myocytes. *Front Physiol* 2012;**3**:174.

21. Fenske S, Hennis K, Rötzer RD, Brox VF, Becirovic E, Scharr A, Gruner C, Ziegler T, Mehlfeld V, Brennan J, Efimov IR, Pauža AG, Moser M, Wotjak CT, Kupatt C, Gönner R, Zhang R, Zhang H, Zong X, Biel M, Wahl-Schott C. cAMP-dependent regulation of HCN4 controls the tonic entrainment process in sinoatrial node pacemaker cells. *Nat Commun* 2020;**11**:5555.

22. Bidaud I, Chong ACY, Carcouet A, Waard SD, Charpentier F, Ronjat M, Waard MD, Isbrandt D, Wickman K, Vincent A, Mangoni ME, Mesirca P. Inhibition of G protein-gated K$^+$ channels by tertiapin-Q rescues sinus node dysfunction and atrioventricular conduction in mouse models of primary bradycardia. *Sci Rep* 2020;**10**:9835.

23. Shaffer F, Ginsberg JP. An overview of heart rate variability metrics and norms. *Front Public Health* 2017;**5**:258.

24. Shemla O, Tsutsui K, Behar JA, Yaniv Y. Beating rate variability of isolated mammal sinoatrial node tissue: insight into its contribution to heart rate variability. *Front Neurosci* 2020;**14**:614141.

25. Trépanier-Boulay V, St-Michel C, Tremblay A, Fiset C. Gender-based differences in cardiac repolarization in mouse ventricle. *Circ Res* 2001;**89**:437–444.

26. Lizotte E, Tremblay A, Allen BG, Fiset C. Isolation and characterization of subcellular protein fractions from mouse heart. *Anal Biochem* 2005;**345**:47–54.

27. Lomax AE, Rose RA, Giles WR. Electrophysiological evidence for a gradient of G protein-gated K$^+$ current in adult mouse atria. *Br J Pharmacol* 2003;**140**:576–584.

28. Lyashkov AE, Vinogradova TM, Zahanich I, Li Y, Younes A, Nuss HB, Spurgeon HA, Maltsev VA, Lakatta EG. Cholinergic receptor signaling modulates spontaneous firing of sinoatrial nodal cells via integrated effects on PKA-dependent Ca^{2+} cycling and IKACh. *Am J Physiol Heart Circ Physiol* 2009;**297**:H949–H959.

29. Wickman K, Nemec J, Gendler SJ, Clapham DE. Abnormal heart rate regulation in GIRK4 knockout mice. *Neuron* 1998;**20**:103–114.

30. Mesirca P, Marger L, Toyoda F, Rizzetto R, Audoubert M, Dubel S, Torrente AG, DiFrancesco ML, Muller JC, Leoni A-L, Couette B, Nargeot J, Clapham DE, Wickman K, Mangoni ME. The G-protein–gated K$^+$ channel, IKACh, is required for regulation of pacemaker activity and recovery of resting heart rate after sympathetic stimulation. *J Gen Physiol* 2013;**142**:113–126.

31. Posokhova E, Ng D, Opel A, Masuho I, Tinker A, Biesecker LG, Wickman K, Martemyanov KA. Essential role of the m2R-RGS6-IKACh pathway in controlling intrinsic heart rate variability. *PLoS One* 2013;**8**:e76973.

32. Tiwari R, Kumar R, Malik S, Raj T, Kumar P. Analysis of heart rate variability and implication of different factors on heart rate variability. *Curr Cardiol Rev* 2021;**17**:e160721189770.

33. Yaniv Y, Lyashkov AE, Lakatta EG. Impaired signaling intrinsic to sinoatrial node pacemaker cells affects heart rate variability during cardiac disease. *J Clin Trials* 2014;**4**:152.

34. Green LJ, Pullon R, Mackillop LH, Gerry S, Birks J, Salvi D, Davidson S, Loerup L, Tarassenko L, Mossop J, Edwards C, Gauntlett R, Harding K, Chappell LC, Knight M, Watkinson PJ. Postpartum-specific vital sign reference ranges. *Obstet Gynecol* 2021;**137**:295–304.

35. Kuß J, Stallmeyer B, Goldstein M, Rinné S, Pees C, Zumhagen S, Seebohm G, Decher N, Pott L, Kienitz M-C, Schulze-Bahr E. Familial sinus node disease caused by a gain of GIRK (G-protein activated inwardly rectifying K$^+$ channel) channel function. *Circ Genom Precis Med* 2019;**12**:e002238.

36. Mesirca P, Bidaud I, Briec F, Evain S, Torrente AG, Le Quang K, Leoni A-L, Baudot M, Marger L, Chung You Chong A, Nargeot J, Striessnig J, Wickman K, Charpentier F, Mangoni ME. G protein-gated IKACh channels as therapeutic targets for treatment of sick sinus syndrome and heart block. *Proc Natl Acad Sci U S A* 2016;**113**:E932–E941.

37. Garg P, Yadav K, Jaryal AK, Kachhawa G, Kriplani A, Deepak KK. Sequential analysis of heart rate variability, blood pressure variability and baroreflex sensitivity in healthy pregnancy. *Clin Auton Res* 2020;**30**:433–439.

38. Kataoka K, Tomiya Y, Sakamoto A, Kamada Y, Hiramatsu Y, Nakatsuka M. Altered autonomic nervous system activity in women with unexplained recurrent pregnancy loss. *J Obstet Gynaecol Res* 2015;**41**:912–918.

39. Grad C. Heart rate variability and heart rate recovery as prognostic factors. *Clujul Med* 2015;**88**:304–309.

40. Kepley JM, Bates K, Mohiuddin SS. *Physiology, maternal changes*. Treasure Island (FL): StatPearls Publishing; 2023.

41. Joglar JA, Kapa S, Saarel EV, Dubin AM, Gorenek B, Hameed AB, de Melo SL, Leal MA, Mondésert B, Pacheco LD, Robinson MR, Sarkozy A, Silversides CK, Spears D, Srinivas SK, Strasburger JF, Tedrow UB, Wright JM, Zelop CM, Zentner D. 2023 HRS expert consensus statement on the management of arrhythmias during pregnancy. *Heart Rhythm* 2023;**20**:e175–e264.